PAPER

Enhancement of phase separation and superconductivity in Mn-doped $K_{0.8}Fe_{2-y}Mn_ySe_2$ crystals

To cite this article: M T Li *et al* 2013 *J. Phys.: Condens. Matter* **25** 335701

J. Phys.: Condens. Matter **25** (2013) 335701 (8pp) doi:10.1088/0953-8984/25/33/335701

Enhancement of phase separation and superconductivity in Mn-doped $K_{0.8}Fe_{2-y}Mn_ySe_2$ crystals

M T Li[1,2], L Chen[1], Z W Li[2], G H Ryu[2], C T Lin[2] and J C Zhang[1,3]

[1] Department of Physics, Shanghai University, Shanghai 200444, People's Republic of China
[2] Max Planck Institute for Solid State Research, Heisenbergstraße 1, D-70569 Stuttgart, Germany

E-mail: jczhang@staff.shu.edu.cn

Received 27 April 2013, in final form 6 July 2013
Published 24 July 2013
Online at stacks.iop.org/JPhysCM/25/335701

Abstract
Single crystals of $K_{0.8}Fe_{2-y}Mn_ySe_2$ with slight Mn doping have been grown by a self-flux method. X-ray diffraction measurements show enhanced phase separation with increasing Mn doping in the compounds. The superconducting transition temperature increases to $T_{c,onset} \sim 46.1$ K for the sample with $y \sim 0.03$, as observed by electrical transport measurements. Our results demonstrate that the doping of Mn does not suppress the superconductivity, and on the contrary increases the superconducting shield fraction and transition temperature, an effect which may originate from the Mn dopant's high preference to fill into iron vacancies in the Mn-doped samples. It suggests that the Mn dopant can induce a local lattice strain or distortion that profitably modifies the microstructure of the superconducting/metallic phase, leading to superconductivity of the compound.

(Some figures may appear in colour only in the online journal)

1. Introduction

Numerous theoretical and experimental works have focused on the iron-based superconducting compounds to elucidate their unconventional superconducting mechanism since their discovery in 2008 [1]. Among these compounds, the simple binary iron chalcogenides $Fe_{1+\delta}$ (Se, Te, S) (11-type) have the simplest structure, with $T_c \sim 8$–15 K [2, 3]. Their T_c can be enhanced up to ~37 K under high pressure and to ~53 K in the form of a single unit cell film [4, 5]. By the intercalation of monovalent ions A (A = K, Rb, Cs or Tl) [6, 7], namely $A_xFe_{2-y}Se_2$, the T_c can be improved to ~30 K. Subsequently, the $A_xFe_{2-y}Se_2$ compound has attracted much interest due to its intriguing physical properties [8, 9].

The existence of intrinsic phase separation in the family of $A_xFe_{2-y}Se_2$ has been evidenced by tunneling electron microscope (TEM) [10], muon spin rotation (μSR) [11], scanning electron microscope (SEM) [12, 13], scanning tunneling microscope (STM) [14], and angle resolved photoemission spectroscopy (ARPES) measurements [15]. The nature of the phase separation indicates that the Fe-vacancy-free $A_xFe_2Se_2$ is responsible for the high-T_c superconductivity and Fe-vacancy-ordered $(\sqrt{5} \times \sqrt{5})$ $A_2Fe_4Se_5$ corresponds to the insulating/semiconducting phase. The superconducting/metallic phase of $K_{0.8}Fe_{2-y}Se_2$ is suggested to form during cooling of $K_2Fe_4Se_5$ at the structure phase transition temperature $T_s \sim 280\,^{\circ}C$, leading to the phase separation, i.e., a Fe-vacancy-ordered/disordered transition [12]. Nevertheless, the intrinsic origin of high-T_c superconductivity in the non-balanced chemical valence $A_xFe_{2-y}Se_2$ compounds is still under debate [8, 9, 16, 17]. According to a recent STM study, Li *et al* suggest that Se vacancies or the interfaces between $K_2Fe_4Se_5$ and KFe_2Se_2 may be the two key factors to induce superconductivity in the parent KFe_2Se_2 metallic compound [17]. Due to the metastable state of the superconducting phase, the superconducting properties could also be irreversibly tuned and improved by a post-annealing and quenching technique [12, 18]. Another way to tune the superconducting property of $A_xFe_{2-y}Se_2$ is to substitute Tl by K and change the Fe content in the range $0 \leq y \leq 0.6$ in

[3] Address for correspondence: Department of Physics, Shanghai University, No. 99 Shangda Road, Shanghai 200444, People's Republic of China.

the $K_{0.8}Fe_{2+y}Se_2$ stoichiometry or $0 \leq y \leq 0.4$ in the $K_{0.8}Fe_{1.6+y}Se_2$ stoichiometry, and a second superconducting phase with T_c above 40 K has been observed [7, 19, 20]. Moreover, Sun *et al* also observed a superconducting transition above 40 K in $A_xFe_{2-y}Se_2$ (A = K, Rb, Tl) under high pressures and proposed the existence of pressure-driven quantum criticality [21, 22].

Very recently, several novel intercalation methods on FeSe have been performed to enhance its T_c above 40 K, such as $A_xFe_2Se_2$ (A = Li, Na, Ba, Sr, Ca, Yb, and Eu) with $T_{c,onset}$ = 30–46 K [23], $Li_x(C_5H_5N)_yFe_{2-z}Se_2$ with $T_{c,onset}$ = 45 K [24], $Li_xFe_2Se_2(NH_3)_y$ with $T_{c,onset}$ = 44 K [25], and $Li_x(NH_2)_y(NH_3)_{1-y}Fe_2Se_2$ ($x \sim 0.6$; $y \sim 0.2$) with $T_{c,onset}$ = 43 K [26]. However, these are polycrystalline powders with some degree of uncertainty regarding the presence of impurity phases, and with very broad superconducting transition widths. Thus, it is hard to interpret the superconducting mechanisms. Intriguingly, it was reported that the superconducting properties of $Fe_{1-y}Mn_yTe_{0.5}Se_{0.5}$ single crystal could be improved by doping the transition metal of Mn with $y \sim 0.02$ [27]. A similar result was also achieved for the doping level of Mn $y < 0.04$ for $A_{0.8}Fe_{2-y}Mn_ySe_2$ single crystals [28, 29], while the opposite effect occurs with other transition metal doping, such as Ni and Co [28–30].

Studies of transition metal doping effects on superconductivity can provide important information on the superconducting mechanism and the pairing symmetry, and it was reported that the effects of doping with Mn and other transition metals on the T_c for intercalated iron selenide superconductors show very contrasting behavior [28–30]. The Mn dopant does not suppress the T_c value while a rapid decrease of T_c was observed in other transition metal doping [28–30]. Furthermore, it was reported that the transition metal doping always suppresses the T_c value in $Ba_{0.5}K_{0.5}Fe_2As_2$ iron arsenic superconductor [31], which has an isotropic structure with the superconducting phase of the $A_xFe_{2-y}Se_2$ compounds. As mentioned before, the existence of intrinsic phase separation may result in inconclusive studies of the effects of transition metal doping on iron selenide superconductors; for instance, it is still unclear how the transition metal dopants are distributed in the phase separated $A_xFe_{2-y}Se_2$ lattice and whether most of them really enter into the superconducting phase or not. For the Mn dopant, the observed non-suppression of T_c leads us to reexamine the role of the effects of Mn doping on the superconductivity and phase separation in the $K_xFe_{2-y}Se_2$ system [28].

In this work, we present the results of Mn-doped $K_{0.8}Fe_{2-y}Mn_ySe_2$ single crystals to elucidate the effects of the Mn dopant on the superconducting properties and phase separation of the compound. It is found that the shielding fraction was significantly enhanced to ~70% for Mn-doped samples as compared to ~12% for non-doped sample, in contrast to a previous result [28]. In the slight Mn doping $y \sim 0.03$ case, the superconducting transition temperature is enhanced up to $T_c \sim 46$ K. The redistribution and precipitation of the superconducting phase was also investigated by post-annealing and quenching treatment, as described in previous reports [12, 18]. The effects of Mn doping and thermal treatment on phase separation and the enhancement of T_c are discussed.

2. Experimental details

Single crystals of $K_{0.8}Fe_{2-y}Mn_ySe_2$ (y = 0, 0.01, 0.02, 0.03) were prepared by a self-flux method [32]. High-purity Fe (99.9%), Se (99.95%), Mn (99.6%) powders were first mixed thoroughly in an Ar filled glove box according to the nominal composition of $Fe_{1-y/2}Mn_{y/2}Se$. The mixed powders were pressed into pellets, and then annealed at 700 °C for 12 h in an evacuated ampule to create the precursors. Then K fragments and $Fe_{1-y/2}Mn_{y/2}Se$ bulks of about 5 g with a molar ratio of 0.8:2 were loaded into an ampule and evacuated. To prevent cracking of the ampule from the high chemical reactivity of potassium, the loaded ampule was sealed into another larger quartz tube and filled with 2–10 Pa Ar. The crystal growth was carried out in a horizontal tube furnace. The mixtures were slowly heated to 1050 °C and soaked for 3 h to get a homogeneous melt, then cooled down to 700 °C at a rate of 5 °C h^{-1} before switching off the power. As-grown crystals with a size of several millimeters were obtained and exhibit shiny surface facets of (0 0 l). For the post-annealing treatment, the samples were sealed in an evacuated ampule, heated to above ~400 °C (higher than $T_s \sim 280$ °C) for 3 h, and subsequently quenched into ice cold water.

The crystal structure was examined by x-ray diffraction (XRD) measurements using a PHILIPS PW3710 diffractometer with Cu Kα radiation. The crystal composition was determined using energy dispersive x-ray spectroscopy (EDX), and a total of nine points for spectroscopy were measured on the freshly cleaved surface of the crystal. The surface topography analysis was performed in a Tescan Vega TS-5130MM scanning electron microscope (SEM) equipped with a NORRAN System 7 UltraDry Detector and a high-resolution Zeiss Crossbeam 1540 EsB SEM for detailed observations of the phase separation features of the samples. In-plane resistance was measured by a physical properties measurement system (PPMS-9, Quantum Design) using the standard four wires with silver paste as the contacts, and DC magnetic susceptibility was measured using a SQUID-VSM magnetometer (Quantum Design), in the temperature range from 2 to 50 K under low magnetic fields of H = 10 Oe for configurations of both field parallel ($H \parallel ab$) and field perpendicular ($H \parallel c$) to the *ab*-plane.

3. Results and discussion

Figure 1(a) shows the crystal structure of the superconducting phase $K_xFe_2Se_2$ without Fe-vacancies, which crystallizes into $ThCr_2Si_2$-like structure, similar to potassium-doped $BaFe_2As_2$ iron arsenic superconductor [31]. A typical crystal with millimeter size and shiny surfaces is shown in the right upper graph, while the lower graph displays its fresh-cleaved surface morphology. Figure 1(b) shows the sketch of insulating/semiconducting phase $K_2Fe_4Se_5$ with Fe-vacancy $\sqrt{5} \times \sqrt{5}$ ordering [8, 9]. That the Mn dopant favors occupying Fe-vacancy sites instead of Fe sites is

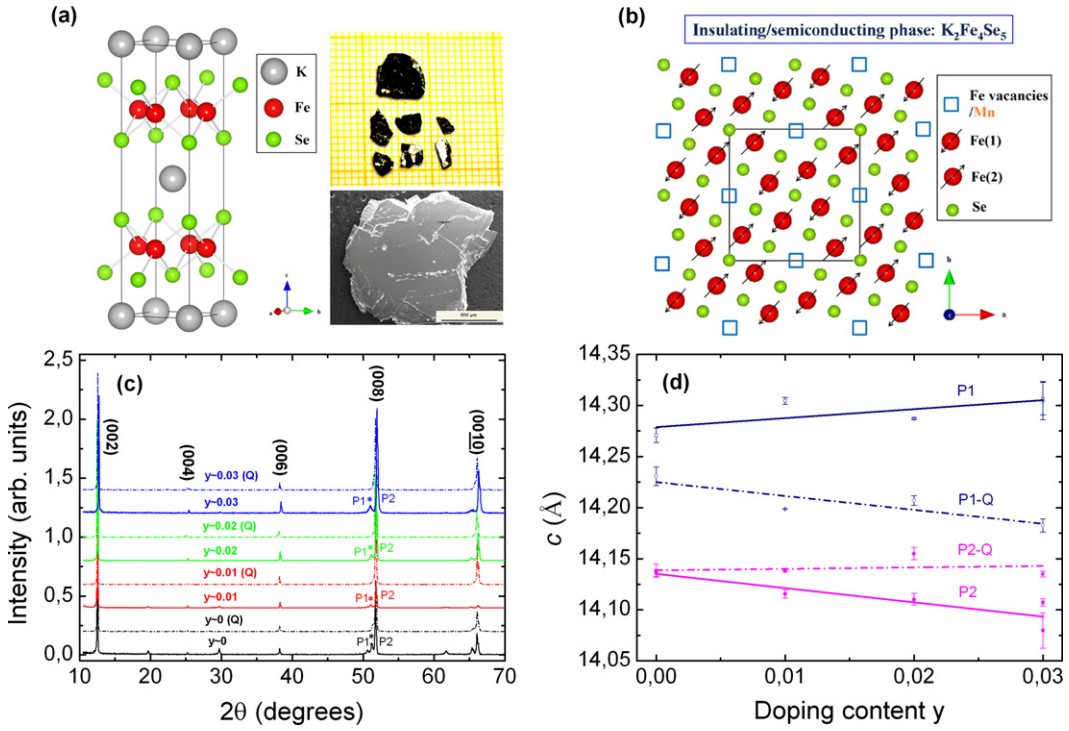

Figure 1. (a) The crystal structure of superconducting phase $K_xFe_2Se_2$ without Fe-vacancies. A typical crystal with millimeter size is shown in right upper graph, while the lower graph displays its fresh-cleaved surface morphology. (b) The sketch of insulating phase $K_2Fe_4Se_5$ with Fe-vacancy $\sqrt{5} \times \sqrt{5}$ ordering. The Mn dopant favors occupying Fe-vacancy sites, as discussed in the text. (c) The (0 0 *l*) XRD patterns for single crystals of $K_{0.8}Fe_{2-y}Mn_ySe_2$ with $y = 0$, 0.01, 0.02 and 0.03, respectively. The solid and dotted lines were obtained from the as-grown and quenched crystals, respectively. P1 and P2 denote the weak and strong reflections, and Q denotes the quenched sample, respectively. (d) The Mn doping dependence of the *c* lattice parameters. The *c* lattice parameters for P1 and P2 are plotted for the as-grown samples, and the P1-Q and P2-Q are plotted for the quenched samples, respectively.

supported from our XRD and transport measurements, which will be discussed in the following paragraphs.

The as-grown single crystals commonly exhibited an intergrowth of the iron-vacancy-ordered and iron-vacancy-disordered states along the *c*-axis, as characterized by slightly different lattice constants. The XRD pattern shown in figure 1(c) was obtained from the (0 0 l) reflections of the as-grown single crystals, consistent with previous results [32]. We define phase 1 (P1) and phase 2 (P2) as corresponding to the weak and strong reflections, respectively. After quenching, the two phases are represented as P1-Q and P2-Q. Shoulders of the weak reflections besides the strong (0 0 8) and (0 0 10) reflections can be observed, as indicated by the asterisks. This second set of weak (0 0 l) reflections is related to the phase separation phenomenon [12, 20, 32]. After quenching the samples, it is noticed that the separation of P1 and P2 tends to decrease and this feature is more pronounced for the doping content of $y \sim 0.03$, as shown in figure 1(c).

Figure 1(d) plots the Mn doping dependence of the *c*-axis lattice parameters for both as-grown and quenched samples. For the as-grown samples, the lattice parameter c_1 increases with increasing Mn doping levels, while the inverse trend happens for c_2, which decreases with increasing Mn. Taking into account the intrinsic phase separation picture supported by the recent reports [10–15, 20, 32], the P1 (asterisks) can be attributed to the superconducting/metallic phase of $K_xFe_2Se_2$ without iron vacancies. On the other hand, since the ionic radius of Mn^{2+} (0.66 Å) is larger than that of Fe^{2+} (0.63 Å), assuming the dopant and host ions adopt the 2+ valence state, the decrease of the c_2 lattice parameters indicates that the Mn dopant highly favors filling into the Fe-vacancy sites of the $K_2Fe_4Se_5$ phase while the increase of c_1 is suggested to originate from compressive strain at interfaces between P1 and P2.

It was noticed that the lattice parameters of P1-Q decreased with Mn doping content after the samples were quenched, indicating that the present superconducting phase partly switched into the insulating phase. Nevertheless, the lattice parameters of P2-Q are nearly independent of the Mn doping, but increase as compared to the as-grown samples. This can be direct evidence of the existence of significant lattice strain in the as-grown samples, which will be released after the post-annealing treatment. The quenched samples show a strong reflection of P2 but a weak reflection of P1, as clearly seen in the (0 0 8) and (0 0 10) peaks in figure 1(c). The change of the *c* lattice parameters can be related to the effect of Mn doping on the structural properties and phase separation, which is attributed to phase redistribution occurring in both superconducting/metallic and insulating/semiconducting phases in the quenched samples. In contrast to the Mn-doped samples, c_1 decreased by about 0.28% while c_2 shows no pronounced change for the non-doped sample. Meanwhile, the reflection of P1 is much stronger than that of P1 for Mn-doped samples, indicating the

superconducting phase can survive well after the quenching treatment, in good agreement with previous results [12]. However, for as-grown Mn-doped samples, c_1 increased by ~0.25%, while c_2 reduced by ~0.22–0.44% for the $y \sim 0.03$ sample, as compared to the pure compound with $y = 0$. The largest c_1 is obtained with a Mn doping content of $y \sim 0.03$, showing the strongest phase separation. Since P1 and P2 are responsible for superconducting and insulating phase, the reflections of P1 and P2 can be the fingerprints of the appearance of superconductivity and the insulating state in $A_{0.8}Fe_{2-y}Se_2$, respectively [20, 32]. This feature is evidenced by the Mn doping evolution of the *c*-axis parameters for the quenched samples, which display a convergence of P1 and P2, accompanying the suppression or vanishing of superconductivity in the Mn-doped $K_{0.8}Fe_{2-y}Mn_ySe_2$ crystals, as shown in figure 1(c).

Based on the above structural observation, the results show the effect of Mn doping, with the enhancement of phase separation between P1 and P2 for the as-grown samples, while convergence of the two phases is observed in the quenched samples, as shown in figure 1(c) and (d). This feature can be directly related to the superconductivity, as evidenced by the magnetic susceptibility and electrical transport data. The details will be described in the following paragraphs.

The DC magnetic susceptibility and resistivity were measured for the as-grown $K_{0.8}Fe_{2-y}Mn_ySe_2$ single crystals, as shown in figures 2(a) and (b), respectively. The first superconducting transition temperature occurs at $T_{c1} \sim 32$ K for all samples, suggesting that the Mn dopant does not suppress the common superconducting transition temperature T_{c1}, in agreement with recent reports [28, 29]. For the non-doped $K_{0.8}Fe_2Se_2$ sample, the superconducting shield fraction (SF) is estimated as about 12% at 2 K. It is interesting to note that the superconducting transition becomes much sharper and the SF significantly increases to 72% for both samples doped with Mn doping of $y \sim 0.01$ and $y \sim 0.02$, respectively. This indicates that slight Mn doping could improve the superconducting properties of the $K_{0.8}Fe_{2-y}Se_2$ compound. Another interesting feature of the enhancement of the second superconducting transition at $T_{c2} \sim 38.0$ and ~42.1 K is also observed for the two samples with Mn of $y \sim 0.01$ and $y \sim 0.03$ from magnetic susceptibility measurements, as indicated in the inset of figure 2(a). The maximum transition temperature occurs at $T_{c2,onset} \sim 46.1$ and $T_{c2,zero} \sim 32.4$ K for $y \sim 0.03$, obtained by electrical transport measurements, as shown in figure 2(b) in the enlarged part in the inset. The second transition of T_{c2} was not observed for the sample with Mn ~ 0.02, but it shows a sharper transition and higher residual resistance ratio RRR = 39.7 compared to 16.8 for the non-doped one, where RRR = $R(T_h)/R(T_{c,onset})$ and T_h is the hump temperature. An improvement of superconductivity was also observed in the Mn-doped $FeTe_{0.5}Se_{0.5}$ iron chalcogenide superconductors [27].

A common feature of the temperature dependence of resistivity curves is the hump peak in the normal state, which is recognized as the synergistic result of electrical transport between the insulating/semiconducting and superconducting

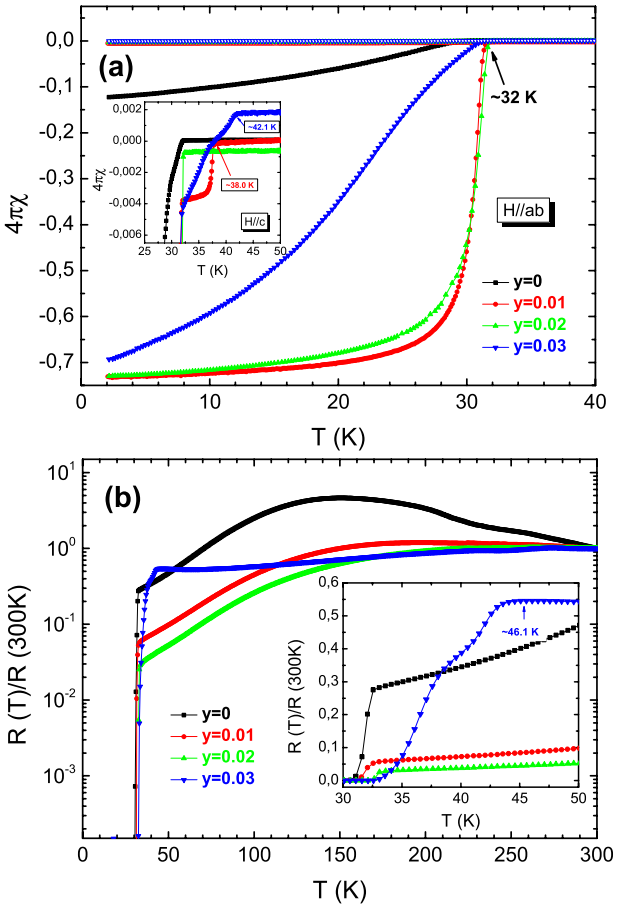

Figure 2. (a) The temperature dependence of magnetic susceptibility with $H = 10$ Oe parallel to the *ab* plane for $K_{0.8}Fe_{2-y}Mn_ySe_2$ single crystals with $y = 0$, 0.01, 0.02, 0.03. The inset displays data near the transition temperature for $H \parallel c$. (b) The temperature dependence of normalized resistance plotted on a log scale. The inset displays a detailed view near the superconducting transition.

/metallic phases [12, 22]. Figure 2(b) shows the hump temperature T_h shifts toward higher temperatures with increasing Mn doping in the as-grown samples. The enhancement of phase separation is more significant for the $y \sim 0.03$ sample, as indicated in figure 1(c) and (d). Therefore, the shift can be directly attributed to the effect of Mn doping on the phase separation. This behavior was also observed for the quenched non-doped sample, as shown in figure 3(a), as also reported by the previous results [12, 18]. An increase of T_h was also observed in a $K_{0.8}Fe_{1.7}Se_2$ sample by inducing an external pressure of <9 GPa [22], above which the superconductivity vanishes. It indicates that the transformation between superconducting/metallic and insulating/semiconducting phases could be driven irreversibly by pressure, which shows the remarkable role of strain in the phase separation behavior of this compound.

In order to further improve the superconducting properties of $y = 0$, 0.01, 0.02 and 0.03 samples, we performed post-annealing and quenching treatment on them at 400 °C for 3 h before quenching them into ice cold water [12, 18]. Figures 3(a)–(d) show the temperature dependence of

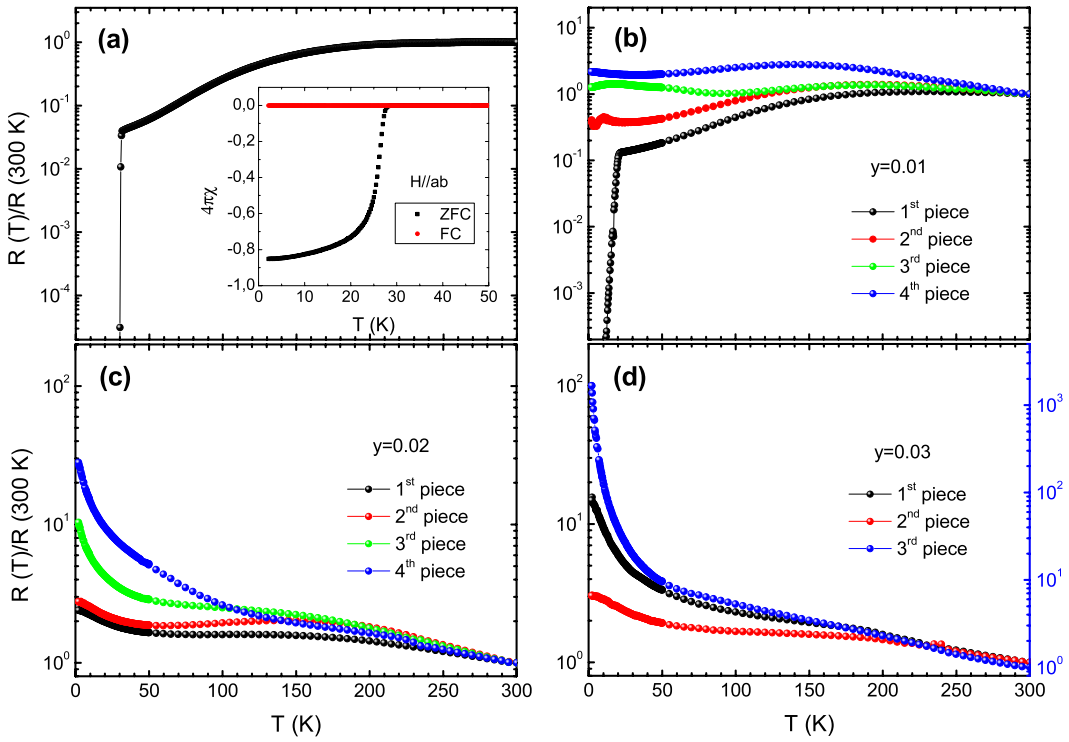

Figure 3. (a)–(d) Temperature dependence of normalized resistivity curves of $y = 0$, 0.01, 0.02 and 0.03 samples after quenching treatment, showing contrasting electric transport behaviors. At least three pieces from different parts of the quenched crystals were selected for electric transport measurements to reveal the common features in Mn-doped samples after quenching treatment.

normalized resistivity for $y = 0$, 0. 01, 0.02 and 0.03 samples after quenching treatment. Intriguingly, the non-doped and Mn-doped samples show remarkably different responses to the thermal treatment. For non-doped sample, it is found that the SF and T_h are significantly improved while a slight lower T_{c1} at 31.6 K is observed from electrical transport measurement, while the superconducting phase is also found to be quite stable, in contrast to a previous result [18], indicating the excess Fe is a necessary factor in the stabilization and precipitation of superconducting phase. Meanwhile, the enhancement of superconductivity for the non-doped sample can be attributed to the modifying precipitation of the superconducting phase driven by the Fe-vacancy order–disorder transition though the quenching process [12]. However, for Mn-doped samples, there is no superconductivity at $T_{c1} \sim 32$ K observed at low temperature, which shows contrasting results compared to the non-doped sample. Moreover, the superconductivity of the $y = 0.02$ and 0.03 samples was completely destroyed by post-annealing and quenching treatment, showing that the superconducting phase is quite metastable to thermal treatment at higher Mn doping content. Nonetheless, for the $y = 0.01$ sample, the resistivity first increases as the temperature is lowered, and then exhibits a broad hump between $T = 140$ and 230 K, below which the metallic state is observed. As the temperature further decreases, we observed a resistivity drop at $T_c = 21.5$ K, 10.5 K, 18.1 K for the first, second, and third experimental samples, respectively. The drop should be associated with the superconducting transition, indicating that the suppression of T_c by the Mn dopant might be exactly realized after post-quenching. However, the superconducting phase is slightly lower than that of as-grown samples, which is responsible for the broad and non-zero resistivity superconducting transition in the quenched samples. Thus, the results provide further evidence on the distribution of Mn dopant, mainly in the insulating/semiconducting $K_2Fe_4Se_5$ phase in as-grown samples, and part of the Mn dopant may freeze in the superconducting $K_xFe_2Se_2$ phase across T_s so as to suppress the T_c [28].

The phase separation in $A_xFe_{2-y}Se_2$ compounds can be directly observed by SEM, TEM and STM techniques [10–14, 20]. The superconducting phase prefers to form stripe-like networks (SNWs) or rectangular bars, as can be seen from SEM images, confirming the percolative superconducting scenario from the transport measurements [33]. The SEM images of figures 4(a)–(d) were obtained from the $y = 0$ and 0.03 samples, and the inset shows the detailed view of the phase separation feature. For the as-grown samples, there are distinct morphologies between non-doped and Mn-doped samples. The non-doped sample always aggregates into disconnected bar chains, as shown in figure 4(a), which show low SF, consistent with previous reports [12, 13]. As seen from figure 4(b), the rectangular bars evolve into well connected SNWs with slight Mn doping in the as-grown samples, while the SF is also remarkably enhanced with a multi-superconducting transition. This result confirms the enhancement of superconductivity by slight doping of Mn in the $K_{0.8}Fe_{2-y}Se_2$ compound. The image of SNWs was also obtained for a non-doped sample after quenching treatment, as shown in figure 4(c). The appearance of these SNWs

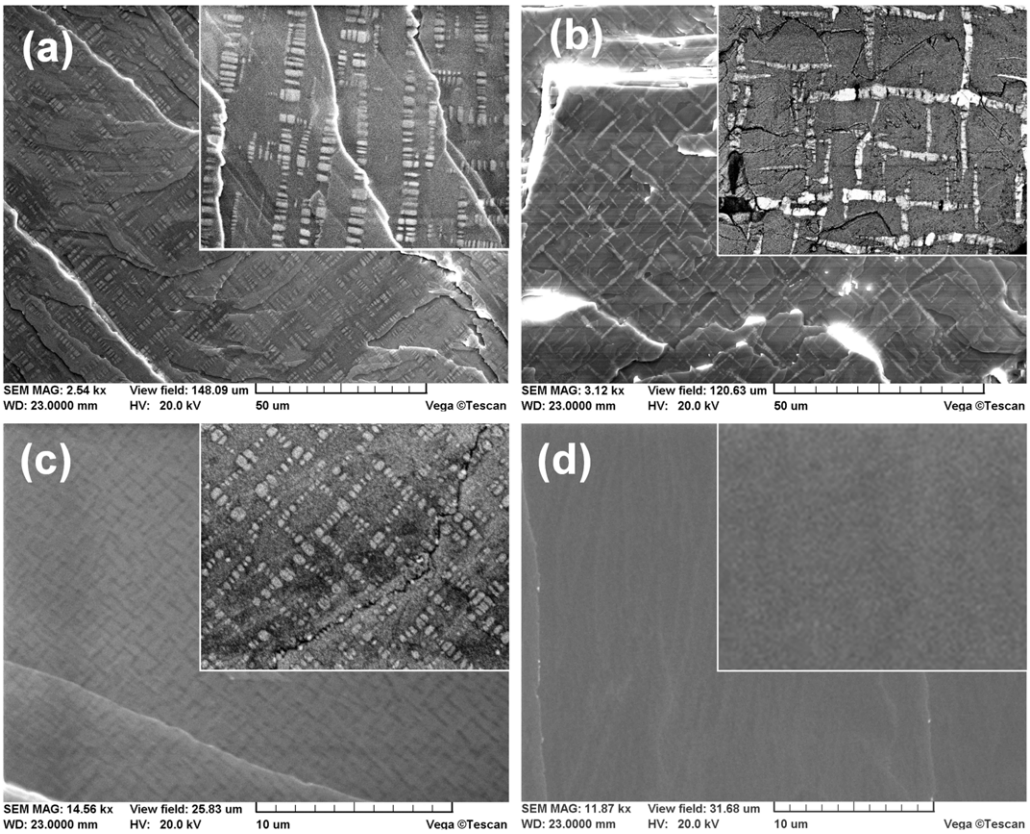

Figure 4. Typical SEM images of the *ab* plane reveal the microstructural modification of the phase separation characteristic in $K_{0.8}Fe_{2-y}Mn_ySe_2$ samples. (a) As-grown, non-doped with rectangular bars, (b) as-grown, $y \sim 0.03$ with pronounced SNWs, (c) quenched, non-doped with fine SNWs and (d) quenched, $y \sim 0.03$ without SNWs.

exhibits a finer and low contrast, as compared to figure 4(a). It indicates that superconductivity was also improved by post-quenching treatment, as proved by our susceptibility and transport measurements (see also [12, 18]) as well as the slightly smaller difference between P1 and P1-Q XRD data in figures 1(c) and (d). After quenching the $y \sim 0.03$ sample, it shows no SNWs, as seen in figure 4(d). Meanwhile, the quenched $y \sim 0.03$ sample lost superconductivity and adopted insulating/semiconducting behavior, as seen in figure 3(d). These results can be directly related to the change of structural data in figure 1(c) and (d), showing the *c*-axis lattice parameter of P1-Q is smaller than that of P1 and the convergence of the P1-Q and P2-Q phases. Consequently, the effect of Mn doping or quenching treatment on the evolution of the *c*-axis parameter can be attributed to phase redistribution in the $K_{0.8}Fe_{2-y}Se_2$ compound.

Comparing to the behavior for doping with other transition metals, figures 5(a) and (b) show the doping dependence of T_c and T_h of $A_{0.8}Fe_2Se_2$ (A = K, Tl) compounds. It can be seen that substitutions of Cr and Co in $K_{0.8}Fe_{2-y}Se_2$ result in a drastic suppression of T_c, while T_c is nearly unchanged in the Mn-doped samples [28, 29]. Our results demonstrate that the Mn dopant can improve and enhance both T_c and T_h in as-grown samples. However, the quenching treatment leads to the suppression of T_c and T_h for Mn-doped samples. Based on the results of thermal treatment and structural evolution, we suggest that the Mn dopant mainly distributes in Fe-vacancy sites of the $K_2Fe_4Se_5$ phase so as to have no pair-breaking effect on T_c in the as-grown samples. Another portion of the Mn dopant can freeze in the Fe sites of the superconducting phase during the structural transition occurring in the quenched samples, resulting in the suppression of T_c. Electron-spin-resonance (ESR) results indicate that Cr and Co induce a large effective magnetic moment, with a much lower effective moment for the Mn ions [28, 29]. Thus, the suppression of superconductivity can be mainly attributed to the magnetic pair-breaking effect for Cr- and Co-doped samples, whereas the reason for the Mn dopant hardly suppressing T_c might be mainly due to the absence of Mn dopant in the superconducting phase, in contrast to the small-angle scattering or small-momentum transfer interpretation [28].

Following the above observations, we would like to propose one alternative scenario for the effect of Mn doping on the phase separation. There are two key factors, namely, thermal history and lattice strain, to determine the phase separation between the $K_2Fe_4Se_5$ phase and the $K_xFe_2Se_2$ phase [12, 34]. Due to different lattice parameters, lattice distortion should exist at interfaces between the two phases and will change with varying temperature [12]. Lattice strain in the $K_2Fe_4Se_5$ phase could prevent the escape of supersaturated Fe from the $K_{0.8}Fe_2Se_2$ solution so as to help the precipitation of the superconducting phase [34]. Meanwhile, the orientation of the superconducting

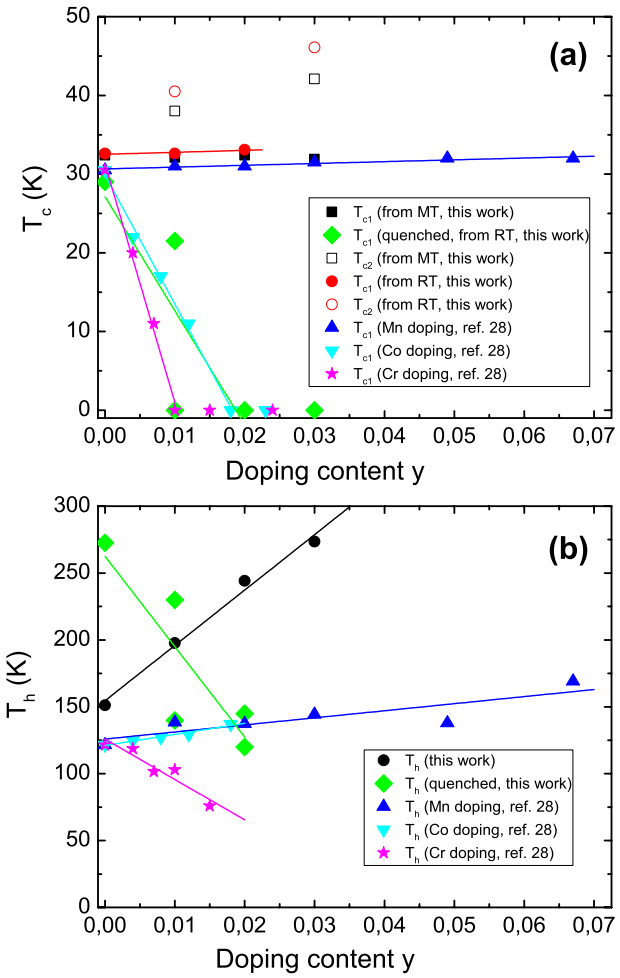

Figure 5. Transition metal doping dependence of T_c (a) and T_h (b) for the $K_{0.8}Fe_2Se_2$ compound. The data on the effects of Mn, Co and Cr doping on $K_{0.8}Fe_2Se_2$ is adapted from [28] for comparison. In our Mn-doped samples, three pieces from different parts of the quenched crystals were selected for resistivity measurements to reveal the common features, although only two typical points are shown for clarity. The solid lines are guides to the eyes.

rectangular bars is suggested to be aligned along the soft elastic strain direction so as to relieve the lattice distortion, while the microstructure of the superconducting phase is determined by the thermal history and interface strain [12, 13, 34]. Thus, the origin of enhancement on the phase separation in slightly Mn-doped as-grown samples could be understood as follows: the Mn dopant induces a large lattice distortion in P1, and the superconducting phase can precipitate to compensate the interface lattice distortion during the moderate cooling process across T_s, which likely forms a network of stripes and induces the superconducting phase with $T_c \geq 32$ K. Nevertheless, for Mn-doped samples, post-annealing above T_s would cause the redistribution of the Mn dopant and the decomposition of the superconducting phase, and it is shown that the superconducting phase cannot form successfully during the fast cooling across T_s by the quenching treatment, in contrast to the non-doped sample. The results indicate that the superconducting phase of Mn-doped samples is more metastable and sensitive to thermal treatment than that of the non-doped sample, similar to metastable polycrystalline $A_xFe_2Se_2$ (A = Li, Na, Ba, Sr, Ca, Yb, and Eu) samples with $T_{c,onset}$ = 30–46 K prepared by the ammonothermal method [23]. Moreover, for Mn-doped as-grown samples, the enhancement of T_h could be understood as the synergetic result of a superconducting $K_xFe_2Se_2$ phase with well-connected networks and an insulating $K_2Fe_4Se_5$ matrix phase.

4. Conclusions

Superconducting $K_{0.8}Fe_{2-y}Mn_ySe_2$ single crystals with slight Mn doping have been prepared by a self-flux method. The doped samples show larger c-axis lattice parameters for the P1 phase in as-grown samples as compared to the non-doped crystals. The highest superconducting transition at $T_{c,onset} \sim 46.1$ K and $T_{c,zero} \sim 32.4$ K was observed for the $K_{0.8}Fe_{2-y}Mn_ySe_2$ with $y \sim 0.03$. Our results show that slight Mn doping does not suppress T_c, and on the contrary enhances the superconductivity. For the as-grown samples, the enhancement of T_c and T_h can be understood as the Mn-dopant's high preference to fill into the Fe-vacancy sites of the insulating/semiconducting $K_2Fe_4Se_5$ phase and the synergistic result of a network connection between the superconducting $K_xFe_2Se_2$ and insulating/semiconducting $K_2Fe_4Se_5$ phases, respectively. For samples quenched above T_s, the superconducting phase was decomposed and a redistribution of the Mn dopant occurred, as confirmed by our transport and SEM measurements. The Mn dopant can induce local lattice strain or distortion in the $K_2Fe_4Se_5$ phase, assisting microstructural modifications and the precipitation of the superconducting phase.

Acknowledgments

The authors would like to thank G Götz for the XRD measurements, B Fenk and C Busch for the SEM measurements. The authors would also like to thank C J Zhang and Y K Li for their help and valuable discussions. This work is supported by the National Natural Science Foundation of China (NSFC, No. 11074163), and the Science and Technology Innovation Fund of the Shanghai Education Committee (No. 12ZZ097).

References

[1] Kamihara Y, Watanabe T, Hirano M and Hosono H 2008 *J. Am. Chem. Soc.* **130** 3296
[2] Hsu F C *et al* 2008 *Proc. Natl Acad. Sci. USA* **105** 14262
[3] Mizuguchi Y, Hara Y, Deguchi K, Tsuda S, Yamaguchi T, Takeda K, Kotegawa H, Tou H and Takano Y 2010 *Supercond. Sci. Technol.* **23** 054013
[4] Medvedev S *et al* 2009 *Nature Mater.* **8** 630
[5] Wang Q Y *et al* 2012 *Chin. Phys. Lett.* **29** 037402
[6] Guo J G, Jin S F, Wang G, Wang S C, Zhu K X, Zhou T T, He M and Chen X L 2010 *Phys. Rev.* B **82** 180520
[7] Fang M H, Wang H D, Dong C H, Li Z J, Feng C M, Chen J and Yuan H Q 2011 *Europhys. Lett.* **94** 27009
[8] Wen H H 2012 *Rep. Prog. Phys.* **75** 112501
[9] Dagotto E 2013 *Rev. Mod. Phys.* **85** 849

[10] Wang Z, Song Y J, Shi H L, Wang Z W, Chen Z, Tian H F, Chen G F, Guo J G, Yang H X and Li J Q 2011 *Phys. Rev.* B **83** 140505
[11] Charnukha A *et al* 2012 *Phys. Rev. Lett.* **109** 017003
[12] Liu Y, Xing Q, Dennis K W, McCallum R W and Lograsso T A 2012 *Phys. Rev.* B **86** 144507
[13] Landsgesell S, Abou-Ras D, Alber D and Prokeš K 2012 *Phys. Rev.* B **86** 224502
[14] Li W *et al* 2012 *Nature Phys.* **8** 126
[15] Chen F *et al* 2011 *Phys. Rev.* X **1** 021020
[16] Yan Y J, Zhang M, Wang A F, Ying J J, Li Z Y, Qin W, Luo X G, Li J Q, Hu J P and Chen X H 2012 *Sci. Rep.* **2** 212
[17] Li W *et al* 2012 *Phys. Rev. Lett.* **109** 057003
[18] Han F, Yang H, Shen B, Wang Z Y, Li C H and Wen H H 2012 *Phil. Mag.* **92** 2553
[19] Wang D M, He J B, Xia T L and Chen G F 2011 *Phys. Rev.* B **83** 132502
[20] Wang Z W, Wang Z, Song Y J, Ma C, Cai Y, Chen Z, Tian H F, Yang H X, Chen G F and Li J Q 2012 *J. Phys. Chem.* C **116** 17847
[21] Sun L L *et al* 2012 *Nature* **483** 67
[22] Guo J *et al* 2012 *Phys. Rev. Lett.* **108** 197001
[23] Ying T P, Chen X L, Wang G, Jin S F, Zhou T T, Lai X F, Zhang H and Wang W Y 2012 *Sci. Rep.* **2** 426
[24] Krzton-Maziopa A, Pomjakushina E V, Pomjakushin V Y, von Rohr F, Schilling A and Conder K 2012 *J. Phys.: Condens. Matter* **24** 382202
[25] Scheidt E W, Hathwar V R, Schmitz D, Dunbar A, Scherer W, Mayr F, Tsurkan V, Deisenhofer J and Loidl A 2012 *Eur. Phys. J.* B **85** 279
[26] Burrard-Lucas M *et al* 2013 *Nature Mater.* **12** 15
[27] Günther A, Deisenhofer J, Kant C, von Nidda H-A K, Tsurkan V and Loidl A 2011 *Supercond. Sci. Technol.* **24** 045009
[28] Tan D *et al* 2011 *Phys. Rev.* B **84** 014502
[29] Yu Y, Zhang C J, Tong W, Zhang L, Tan D, Pi L, Yang Z R, Tian M L, Tan S and Zhang Y H 2012 *New J. Phys.* **14** 023032
[30] Li Y K, Shen C Y, Guo H J, Lv C, Yang X J, Zhang L, Luo Y K, Cao G H and Xu Z A 2012 *J. Phys.: Condens. Matter* **24** 232202
[31] Li J *et al* 2012 *Phys. Rev.* B **85** 214509
[32] Luo X G *et al* 2011 *New J. Phys.* **13** 053011
[33] Shen B, Zeng B, Chen G F, He J B, Wang D M, Yang H and Wen H H 2011 *Europhys. Lett.* **96** 37010
[34] Shoemaker D P, Chung D Y, Claus H, Francisco M C, Avci S, Llobet A and Kanatzidis M G 2012 *Phys. Rev.* B **86** 184511